

IMPROVED METHODS FOR MODELLING IMPERFECTIONS FOR BUCKLING ANALYSIS OF COMPOSITE CYLINDRICAL SHELLS

Jendi Kepple^{*,**}, Gangadhara Prusty^{*}, Garth Pearce^{*}, Donald Kelly^{*}, Rodney Thomson^{*,**,**}

^{*}School of Mechanical and Manufacturing Engineering, The University of New South Wales, Sydney, Australia, ^{**}Cooperative Research Centre for Advanced Composite Structures, Melbourne, Australia, ^{***}Advanced Composite Structures Australia Pty Ltd, Melbourne, Australia.

Keywords: *stochastic analysis, robust design, spectral analysis, buckling, composites*

Abstract

Carbon-fibre reinforced polymer (CFRP) cylindrical shells are used in a variety of aerospace applications. Such shells are extremely imperfection sensitive [1, 2] and feature a large scatter in buckling load levels induced from imperfections introduced in their manufacturing process.

This paper aims to improve the stochastic modelling of cylindrical thickness imperfections in order to better replicate the stochastic variation of the actual thickness and material imperfections for FE analysis.

These results will reduce the cost of producing and aid in improving the design and reliability of newly designed and untested cylinders by accurately modelling thickness and material imperfections for improved stochastic analysis and robust design.

1 Introduction

There is a substantial requirement for more robust, lighter and cheaper launch vehicle structures. Essential to the fabrication of launch vehicle airframes are unstiffened composite shells, which are prone to buckling and are highly sensitive to imperfections which arise during the manufacturing process. These imperfections facilitate the drastic variation of

the actual buckling load from the buckling load of the geometrically perfect structure [1, 2].

The current design guidelines for imperfection sensitive shells are based on the NASA-SP 8007 [3] which dates from 1968 and is only concerned with the design capabilities of isotropic shells. The guideline predicts the reduced buckling load of a given cylinder design by first calculating the theoretical buckling load of a geometrically perfect structure by performing a linear bifurcation analysis using closed-form equations. This theoretical buckling load is then reduced by applying an empirical knockdown factor to account for the differences between theory and experiment.

From recent literature [4-6], the NASA-SP 8007 knockdown factors used in the design of aerospace-quality shell structures were determined to be exceedingly conservative and unsuitable for shells constructed from modern manufacturing processes and materials such as composites. Such a conservative approach means that structures are therefore heavier and more costly than need be.

Dependable and verified design criteria for thin-walled cylindrical shells are required, particularly for shells constructed from advanced materials and manufacturing techniques. 'New Robust DESign Guideline for

Imperfection Sensitive COmposite Launcher Structures' (DESICOS) was established in 2012 and currently receives funding from the European Commission to develop the "Single Perturbation Load Approach" - a new methodology which is being paired with the stochastic approach for improved design criteria of composite shells in buckling [7].

The research conducted for this paper fits under the umbrella of 'stochastic approaches' for the DESICOS project. Stochastic analysis using metamodels [6, 8-12] have proven to be an excellent method for determining the sensitivity of the buckling load of thin shells to various imperfection types. The stochastic analysis of such shells aims to determine the influence of initial shell-wall geometric, thickness and material imperfections and non-uniform applied end-loads on the axial buckling load for improved robustness and reliability.

1.1 Background

Recent work on stochastic analysis of shells to date include Hilburger and Starnes [13], which compared the effect of measured thickness imperfections, lamina fibre volume fraction and applied load distribution for upper and lower bound buckling curves on cylinders with three different lay-ups. The thickness imperfections were varied based on the accuracy tolerances of the coordinate measurement device. Along with varying other initial input parameters, Alfano and Bisagni [14] superimposed axisymmetric buckling modes to model various geometric imperfections.

For geometric imperfections, the method of separation in conjunction with the spectral representation method has previously been used to generate new geometric imperfections on both isotropic [15] and orthotropic [8-10] cylinders for stochastic analysis and robust design.

Geometric imperfections, in this case, are treated as random fields. In Broggi and Schueller [8], the evolutionary power spectra of the geometric imperfections were estimated and

utilised by the spectral representation method to generate a hundred cylinders with geometric imperfections that conform to the statistical limits of the original experimentally tested shells.

For material imperfections, Broggi and Schueller [9] developed a modelling algorithm; an improvement of the Window Moving Averaging Technique, that maps material imperfections onto discrete finite element (FE) points by categorising existing thickness imperfections. The average thickness of each shell was used as the overall thickness of their FE models [8-11] as is the case with other simulations [16].

For composite cylinders manufactured via hand layup, it is widely believed that geometric imperfections arise mainly from imperfections in the mandrel [6]. Hilburger et al. [4] measured initial geometric imperfection data to determine a manufacturing-process-specific imperfection signature for CFRP shells. Thickness imperfections, however, are widely believed to arise mainly from imperfections in the resin distribution and ply gaps and overlaps [8-10]. These different imperfection types make it difficult to replicate thickness imperfections for stochastic analysis due to their differing statistical properties. Indeed, Broggi and Schueller [8] only use the initially measured cylindrical thickness imperfections for their stochastic analysis; relying on the stochastically varying geometric imperfections for further statistical variation.

1.2 Aims

This paper aims to improve the stochastic modelling of thickness imperfections in order to better replicate stochastic variation of the actual thickness in FE analysis. The improved stochastic thickness imperfections may also be used as inputs to the improved Moving Window Averaging Technique [8-10] to improve FE modelling of material imperfections.

In this paper, the power spectrum of thickness imperfections of composite cylinders will be

accurately estimated which will also take into account ply gaps and changes in the distribution of the resin or, in other words, matrix. This spectrum can then be used to further generate additional stochastic results using the spectral representation method [15] for the robust design of thin shelled structures.

An imperfection database of eight nominally identical CFRP IM6/8557 UD ultrasonic scanned and tested cylinders (denoted Z15-Z26) was acquired from a joint DLR-ESA research program [6]. The nominal properties of these cylinders are shown in Table 1.

Table 1. Nominal properties of DLR cylinders.

Property	Nominal Data
Total length (mm)	540
Free length (mm)	500
Radius (mm)	250
Total Thickness (mm)	0.5
Lay up	[±24/±41]
Ply Thickness (mm)	0.125
Cylinder mass (g)	641

The DLR tested cylinders are representative of imperfection sensitive design in which the sensitivity of the axial buckling load to each imperfection type is magnified. The thickness imperfection readings are available as a collection of pixels, where each pixel is identified by one thickness measurement. The thickness values are discrete, and the approximate number of pixels used in each measurement is 513 in the circumferential direction and 183 in the axial direction leading to a total number of 93,769 pixels. The spacing between in the pixels in the circumferential direction is 3.11mm and 2.87mm in the axial direction.

The primary steps involved in estimating the power spectrum of the thickness imperfections and accurately modelling new imperfections for stochastic analysis involve separating the ply gaps and overlaps from variations in the matrix of the eight nominally identical cylinders [6] by means of a Hough transform [18].

The next step involves the use of the 1D STFT to determine which power spectrum estimation method is suitable for estimating variations in the matrix imperfections. The power spectrum is defined as the Fourier transform of the autocorrelation function of a random field [13, 16]. The power spectrum can intuitively be recognised as the distribution of the mean square of the random field over the space-frequency domain [13] as presented in Equation 1:

$$E[|f(x)|^2] = 2 \int_0^{\infty} S(\omega, x) d\omega \quad (1)$$

The power spectrum $S(\omega)$ is called homogeneous if it depends only on frequency, and is called evolutionary $S(\omega, x)$ if depends on frequency ω and spatial localisation x . The periodogram in Equation 1 can be expanded and improved to accurately estimate the random field in question. Methods of estimating the power spectrum include the short-time Fourier transform (STFT) [19], the harmonic wavelet transform [20] and the method of separation [21] among other methods.

Next, a Monte Carlo analysis will be used to generate ply gap imperfections and the spectral representation method will be used to generate new realisations of resin distribution imperfections. The results from the Monte Carlo analysis for the ply gaps will be superimposed onto the results from the spectral representation method in order to provide new stochastic inputs that are accurate in describing changes in the thickness distribution due to ply gaps, overlaps and unevenness in the resin.

In the future, the thickness models can be incorporated into a finite element (FE) analysis and compared with tested results. This novel method of estimating thickness imperfections may lead to FE models which calculate the reduction in the buckling load of cylindrical shells more accurately when compared with previous estimation techniques.

2 The Hough Transform

Thickness imperfections on composite shell structures can generally be attributed to two different causes: by variation in the resin distribution and by incomplete or excessive coverage of plies on the surface resulting in ply gaps or overlaps [8-10]. The angles of these gap lines coincide with the lay-up angles of the plies. When one observes the variation of thickness in the shell structure as shown in Figure 1, one will notice lines of the deepest imperfections which are due to ply gaps and large patches where the overall thickness of a region changes which can be attributed to changes in the resin or matrix distribution. Due to these two distinct imperfection types, it is unlikely that any spectrum estimation method will accurately capture and be able to replicate these imperfections for stochastic analysis due to their variation in statistical properties.

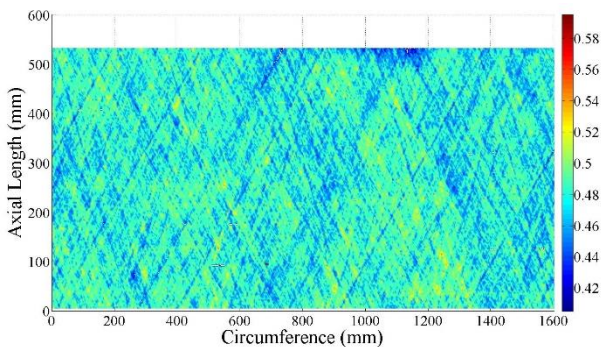


Fig. 1. Ultrasonic-scanned real thickness imperfections on the Z23 cylinder. [6]

The Hough Transform will therefore be used to isolate the ply gaps and overlaps. The ply gaps will be withdrawn from the matrix and statistical measurement tools can be implemented on each imperfection type separately.

The Hough Transform is a feature detection method, which, in this specific case, can be used to detect lines of lowest or highest thickness points which correspond to ply gaps or overlaps [17]. We scan through the Cartesian coordinates of lowest and highest thickness points and assign a “distance to origin” and “angle from origin” of each point via the polar representation shown in Equation 2.

$$r = x \cos \theta + y \sin \theta \quad (2)$$

Where r is the perpendicular distance to the origin and θ is the angle from the positive x -axis to the perpendicular line as described in the Figure 2.

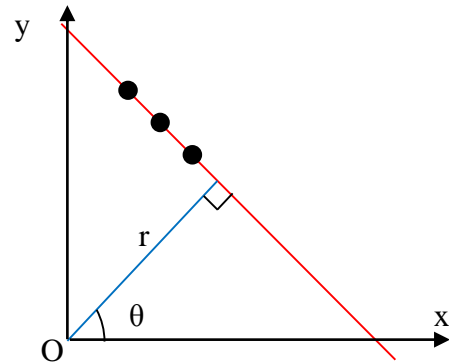


Fig. 2. Polar representation variables of the Hough Transform.

A MATLAB code was devised to determine if a sufficient number of points contain the same perpendicular distance and angle, given a very minor margin of disparity, and then recognized the points as ply gaps or overlaps. These data points were withdrawn from the matrix imperfections and isolated into another data set for further analysis later on.

Figures 1 and 4 show the Z23 and Z26 cylinders (respectively) ultrasonic measured thickness imperfections [6]. The thickness imperfections with the deepest lines are removed (thought to be ply gaps in this case) and are shown in Figure 3 for the Z23 cylinder. Figure 5 features the points that were removed from the Z26 cylinder. The thickness scale is shown on the right hand side of these figures.

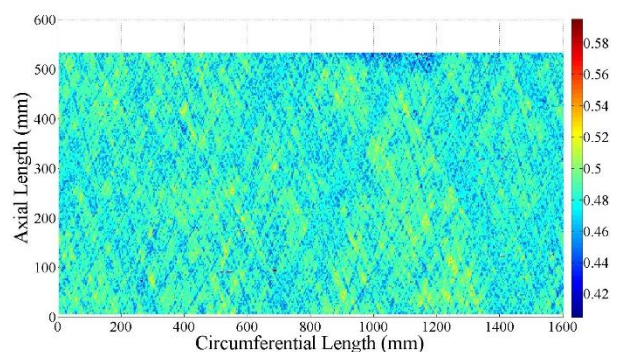


Fig. 3. Z23 cylinder matrix-only imperfections. [6]

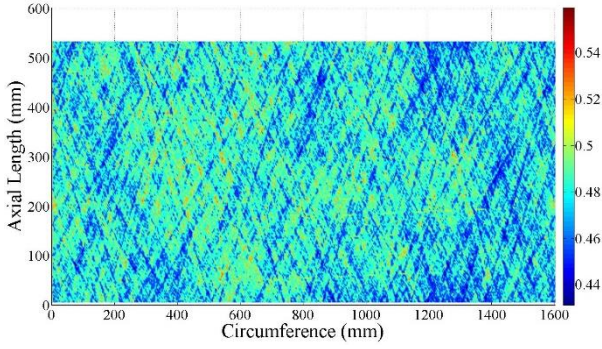


Fig. 4. Z26 cylinder thickness imperfections. [6]

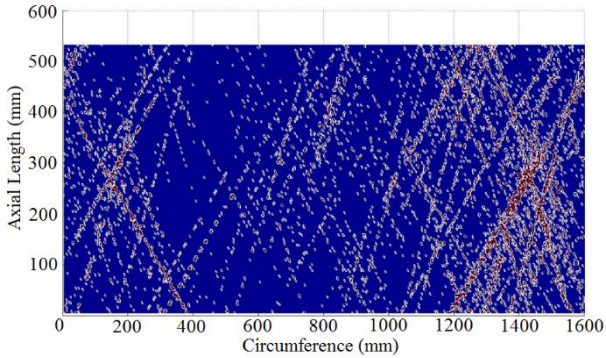


Fig. 5. Points of lowest thickness that were removed from Z26 cylinder. [6]

3 Validation of Stochastic Code

In order to validate the MATLAB codes for obtaining the power spectrum of the thickness imperfections from various spectrum estimation tools, we utilise a 1D benchmark spectrum known as the Kanai Tajimi spectrum [21], which is defined by the equation below by its separable components [22]:

$$S(\omega) = \frac{1 + 4\zeta^2 \left(\frac{\omega}{\omega_0}\right)^2}{\left[\left(1 - \left(\frac{\omega}{\omega_0}\right)^2\right)^2 + \left(2\zeta \frac{\omega}{\omega_0}\right)^2\right]} \quad (3)$$

$$g(x) = \frac{e^{-0.25x} - e^{-0.5x}}{0.25} \quad (4)$$

Where the parameters $\omega_0 = 10\text{rad/mm}$ and $\zeta = 0.24$ represent the natural frequency and the damping ratio, respectively. The exact Kanai Tajimi spectrum is shown in Figure 6.

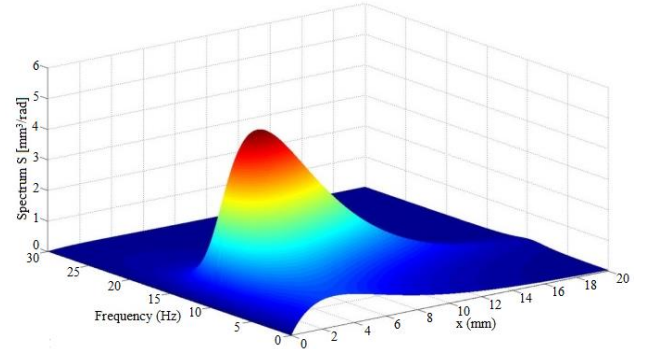


Fig. 6. Exact Kanai Tajimi Spectrum

The spectral representation method for a 1D Gaussian random field was utilised to obtain the stochastic input for the power spectrum estimations. The spectral representation method for a zero-mean 1D Gaussian random field is shown in Equation 5 [17].

$$f^{(i)}(x) = \sqrt{2} \sum_{n=0}^{N-1} A_n \cos(\omega_n x + \phi_n^{(i)}) \quad (5)$$

Where:

$$\begin{aligned} A_n &= \sqrt{2 \cdot S(\omega_n, x) \cdot \Delta\omega} \\ \omega_n &= n \cdot \Delta\omega \\ \Delta\omega &= \omega_{up}/N \\ A_0 &= 0 \text{ or } S(\omega_0 = 0, x) = 0 \end{aligned}$$

Where $i = 0, 1, 2 \dots m$ and $n = 0, 1, 2 \dots (N-1)$ and N determines the discretisation within the active frequency range. ω_{up} is the cut-off frequency, beyond which the spectrum is considered to be zero. $\phi_n^{(i)}$ is the $(i)^{\text{th}}$ realisation of N independent phase angles that are uniformly distributed in the range $[0, 2\pi]$. The spectral estimation techniques used to estimate the Kanai Tajimi spectrum are described as follows.

3.1 1D Method of Separation

The 1D method of separation is considered to be an evolutionary spectrum estimation technique because it focuses on spectrum variations in both the frequency and spatial axes. An evolutionary power spectrum can be considered separable if it can multiplicatively be decomposed into a homogenous spectrum $S(\omega)$

and a modulating envelope $g(x)$ as shown in Equation 6 [15, 17, 22].

$$S(\omega, x) = S_h(\omega) \cdot g(x) \quad (6)$$

The homogenous component of the above separable equation can be estimated using the periodogram [16, 23] displayed in Equation 7.

$$\tilde{S}_h(\omega) = E \left[\frac{1}{2\pi L} \cdot \left| \int_0^L f^{(i)}(x) \cdot e^{-i\omega x} dx \right|^2 \right] \quad (7)$$

From the derivation provided in [9], the modulating envelope can be estimated by the equation shown in Equation 8.

$$g(x) = \frac{E \left[|f^{(i)}(x)|^2 \right]}{2 \int_0^\infty \tilde{S}_h(\omega) d\omega} \quad (8)$$

To use the method of separation, the input samples $f^{(i)}(x)$ need to be approximately separable as the frequency and spatial components must be broken down and dealt with separately. The method of separation based spectrum estimation of the Kanai Tajimi spectrum is shown in Figure 7 for $N = 1000$ showing very accurate variations in both the spatial and frequency axes.

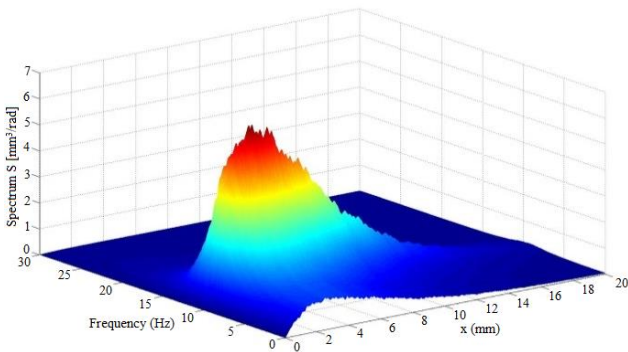


Fig. 7. Method of separation estimation of the Kanai Tajimi spectrum.

3.2 1D Short time Fourier Transform

A common approach for evolutionary power spectrum estimation is by using the STFT method. The STFT emphasises the spectrum at specific spatial locations ($x = \chi$) also known as windows, and suppresses spectrum components that are located further away. The 1D STFT

evolutionary power spectrum estimate is shown in Equation 9 [17].

$$\tilde{S}_j(\omega, x) = E \left[\frac{1}{2\pi T} \cdot \left| \int_{\chi-T/2}^{\chi+T/2} f^{(i)}(x) w(x - \chi^j) \cdot e^{-i\omega x} dx \right|^2 \right] \quad (9)$$

A non-overlapping simple rectangular window function will be used for all estimations in this paper:

$$w(x) = \begin{cases} 1 & -T/2 \leq x \leq T/2 \\ 0 & \text{elsewhere} \end{cases}$$

The STFT based estimate of the Kanai Tajimi spectrum was calculated at 16 equally spaced positions by a non-overlapping rectangular window [15]. Due to the uncertainty principle, a limitation of the STFT is its inability to achieve simultaneous localisation in both frequency and space [19]. If the width of the window is reduced to achieve greater accuracy in the spatial axes, the STFT will sacrifice information in the frequency axes. Similarly, if the width of the window is increased, one would achieve more accurate estimation readings in the frequency component while reducing the precision of information in the spatial axes. In this paper, a compromise in the spatial localisation of the window function has been chosen, that allows for fair localisation in the space without distorting the frequency localisation too severely.

The Kanai Tajimi random field power spectrum estimation using the short time Fourier transform are shown in the Figure 8.

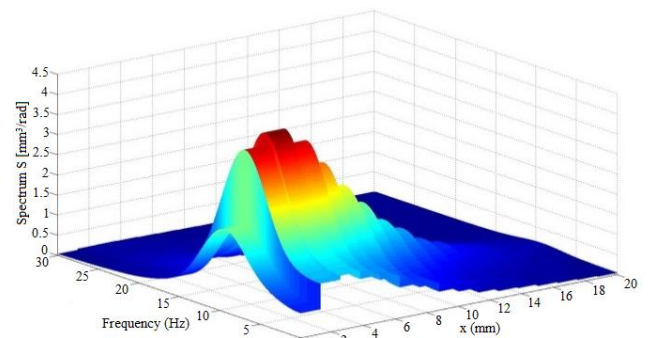


Fig. 8. STFT estimation of the Kanai Tajimi spectrum.

From comparing Figures 6-8, it is clear that the method of separation provides the most accurate spectrum estimate of the Kanai Tajimi spectrum. It has also been used to estimate the evolutionary power spectrum of geometric imperfections in shells [8-10, 15]. It is therefore preferable to model the spectrum of the matrix imperfections by using the method of separation, provided the matrix imperfections fit within the criteria required to use this particular method.

4 Spectral Analysis of Matrix Imperfections

The 1D Short Time Fourier Transform (STFT) is used to determine if the power spectra of the matrix imperfections are suitable for use in the 2D method of separation. If the matrix imperfections are deemed unsuitable, alternative 2D spectrum estimation methods must be implemented.

4.1 1D Short Time Fourier Transform

To use the method of separation as an approximation, one must prove that the imperfections are separable. The criterion of separability strongly depends on the narrow-bandedness of the spectrum; where variations of energy distribution in the frequency domain are considerably limited to a specified frequency range. The bulk of the spectrum within the limited frequency range usually contains 95-100% of the signal to avoid significant estimation errors. Furthermore, the distribution in the spatial axis must be approximately uniformly modulated and must not vary significantly. The spectrum must be calculated about a Gaussian zero mean to be accurate [15].

The 1D Short Time Fourier Transform (STFT) based estimate obtained at 6 equally spaced positions by a non-overlapping rectangular window of length $L/6$ (where L is the circumference of the cylinder) will be used to estimate the extent of the narrow-bandedness of the thickness imperfections to ensure reduced errors in utilising the 2D method of separation. A non-overlapping simple rectangular window function will be used for this estimation [15].

The 1D STFT based spectrum components of the mid-axial-length thickness imperfection measurements in the circumferential direction $f^{(i)}(x)$ (without the removal of any ply gaps) of the Z15-Z26 cylinders [6] is shown in Figure 9(a) and with a side view of their corresponding frequencies shown in Figure 9(b).

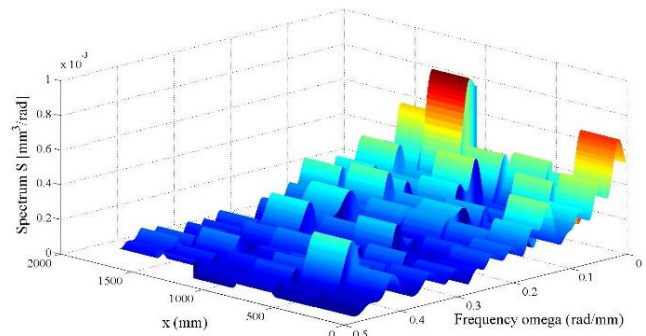


Fig. 9(a). STFT spectrum estimate for mid-axial-length circumferential reading of Z15-Z26 cylinders.

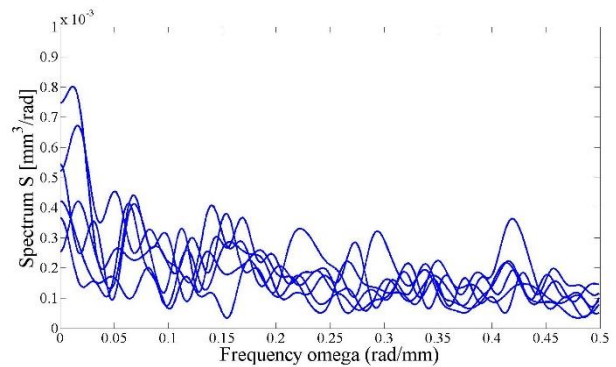


Fig. 9(b). Frequency-side view of STFT spectrum estimates for mid-axial-length circumferential reading of Z15-Z26 cylinders.

As shown in Figures 9(a) and (b), approximately 40% of the variation of the energy distribution in the frequency component is limited to small fixed bandwidth (between 0-0.05rad/mm). A large section of the energy distribution is still represented by the remaining frequencies. Furthermore, 1D STFT based estimates of the lower-most and top-most circumferential readings showed similar trends. This distribution of energy is not sufficient to warrant the use of the method of separation which requires around 95% or more of the main lobe of the energy distribution to be located within a small band-width to avoid large distribution errors [22].

When ply-gap imperfections are removed, there is no improvement to the STFT spectrum estimate in terms of the narrow-bandedness or separability for variations in the matrix. The main lobe contains less than 40% of the energy distribution for the mid-axial-length circumferential imperfection readings as shown in Figures 10(a) and (b).

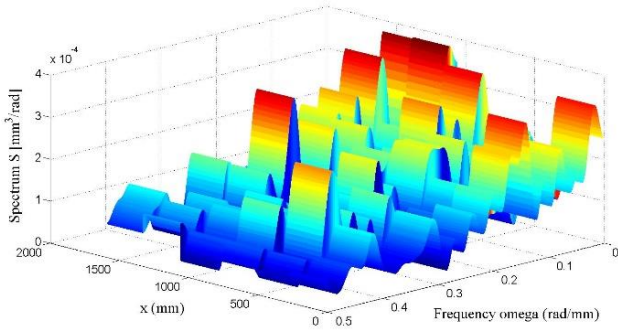


Fig. 10(a). STFT spectrum estimate for mid-axial-length circumferential imperfection readings for Z15-Z26 cylinders with ply gaps removed.

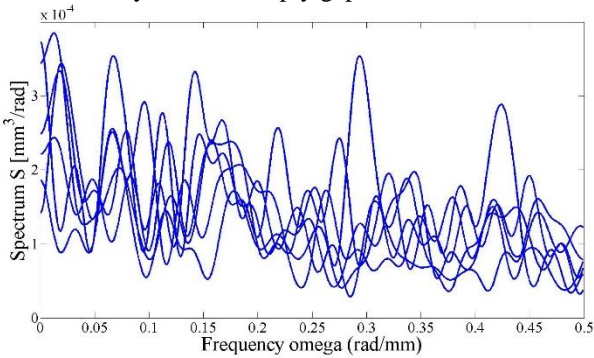


Fig. 10(b). Frequency-side view of STFT spectrum estimates for mid-axial-length circumferential reading of Z15-Z26 cylinders with ply gaps removed.

This indicates that the distributions in the matrix imperfections of the cylinder are largely random and contain very few patterns. Furthermore, the variations in the spatial direction are not uniformly modulated and diverge strongly. Therefore a 2D spectral estimation technique such as the method of separation is unsuitable for this type of imperfection and alternative methods should be sought such as the 2D STFT. The assumption of separability may be worked-around by partitioning the space-frequency spectrum into parts that are of themselves narrow-banded or approximately separable [17]. However, viewing the spectrum estimates as shown in Figures 10(a) and (b), indicates that the spectrum would have to be partitioned into approximately 60 different parts. Each part must then be analysed by the method of separation and then stitched back together to form the complete spectrum. The time and effort required to construct the final spectrum would outweigh any inaccuracies produced by the time-saving 2D STFT method.

4.2 2D Short Time Fourier Transform

The 2D STFT will now be derived and applied to the matrix imperfections in order to estimate the evolutionary power spectrum for stochastic analysis. To expand the 1D STFT to a 2D case, we derive the 2D case from the generalised homogenous periodogram [13] shown in Equation 10.

$$\tilde{S}_{ii}^h(\omega) = E \left[\frac{1}{(2\pi)^2 L_1 \cdot L_2 \dots L_n} \cdot \left| \int_0^{L_1} \dots \int_0^{L_n} f^{(i)}(x) \cdot e^{-i(\omega_n x_n)} dx_n \dots e^{-i(\omega_1 x_1)} dx_1 \right|^2 \right] \quad (10)$$

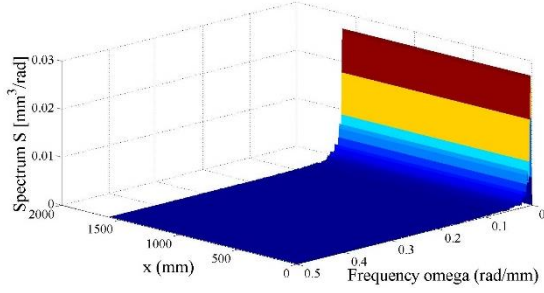
The 2D STFT is therefore:

$$\tilde{S}_j(\omega_1, \omega_2, x, y) = E \left[\frac{1}{4\pi^2 T_x T_y} \cdot \left| \int_{\chi - \frac{T_x}{2}}^{\chi + \frac{T_x}{2}} \int_{\Upsilon - \frac{T_y}{2}}^{\Upsilon + \frac{T_y}{2}} f^{(i)}(x, y) w(x - \chi^j, y - \Upsilon^j) \cdot e^{-i(\omega_1 x + \omega_2 y)} dx dy \right|^2 \right] \quad (11)$$

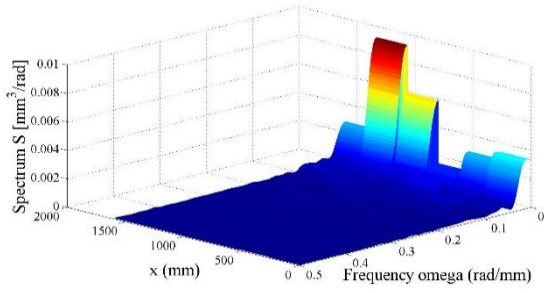
Where x and y correspond to the circumferential and axial directions respectively and T_x and T_y are the widths of the rectangular windowing functions and χ^j and Υ^j correspond to the centre spatial location of the windows to be examined in the circumferential and axial

directions. The 2D STFT was coded into MATLAB and the imperfections due only to changes in the resin distribution of the Z15-Z26 cylinders [6] were added as input functions $f^{(i)}(x, y)$. The resulting 4D function is difficult to plot so the data in the frequency and spatial

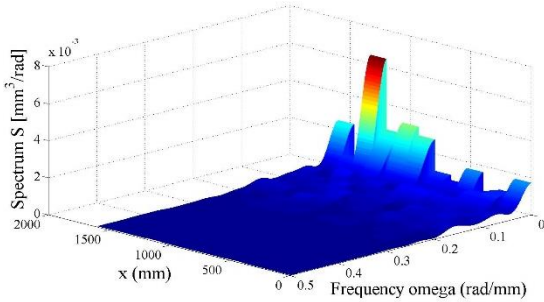
axes in the axial direction have been suppressed for ease of viewing Figures 11(a), (b) and (c).



(a)

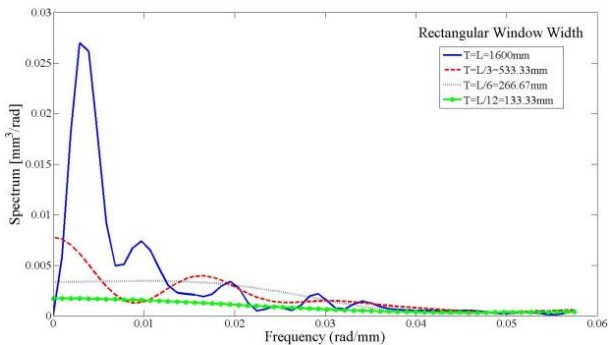


(b)

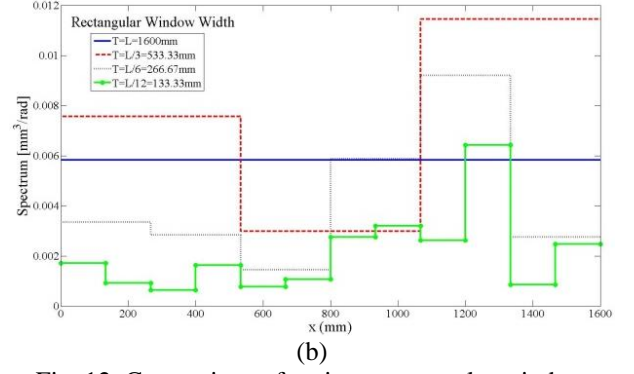


(c)

Fig. 11. 2D STFT of matrix imperfections in the circumferential direction for rectangular window widths (a) $T = L = 1600\text{mm}$, (b) $T = L/6 = 266.67\text{mm}$, (c) $T = L/12 = 133.33\text{mm}$.



(a)



(b)

Fig. 12. Comparison of various rectangular window widths for 2D STFT in the circumferential direction only (axial values suppressed for ease of viewing), (a) reduction in accuracy of frequency estimate with decreasing window size and (b) increase in accuracy of spatial estimate with decreasing window size.

The increase in spatial localisation and the decrease in the accuracy of the frequency data as the window size decreases is a general property of the STFT. This is ‘uncertainly principle’ is motivated from a physical point of view by Heisenberg’s observations in quantum mechanics [22]. It was determined that six rectangular windows would be sufficient to capture the distribution of energy along the spatial axes without substantially damaging the data along the frequency axis.

4.3 Spectral Representation of Matrix Imperfections

Similar to the spectral representation method of the 1D Gaussian random field, the spectral representation for a 2D Gaussian random field is shown in Equation 12 [15].

From Equation 12:

$$A_{nm} = \sqrt{2} \cdot S(\omega_{1n}, \omega_{2m}, x, y) \cdot \Delta\omega_1 \cdot \Delta\omega_2$$

N_1 and N_2 determine the discretisation within the active frequency range of the circumferential and axial axes. $\phi_1^{(i)}$ and $\phi_2^{(i)}$ are the $(i)^{\text{th}}$ realisations of N_1 and N_2 independent phase angles that are uniformly distributed in the range $[0, 2\pi]$.

$$f^{(i)}(x, y) = \sqrt{2} \sum_{n=0}^{N_1-1} \sum_{m=0}^{N_2-1} \left[A_{nm} \cos(\omega_{1n}x + \omega_{2m}y + \phi_1^{(i)}) + A_{nm} \cos(\omega_{1n}x - \omega_{2m}y + \phi_2^{(i)}) \right] \quad (12)$$

A MATLAB code was devised where the 2D STFT spectrum estimate for matrix imperfections was incorporated into the 2D spectral representation method and produced 100 new realisations of the random field. A few results for this process are shown in Figures 13(a) and (b) and are comparable with original matrix imperfections as shown in Figure 3 [6].

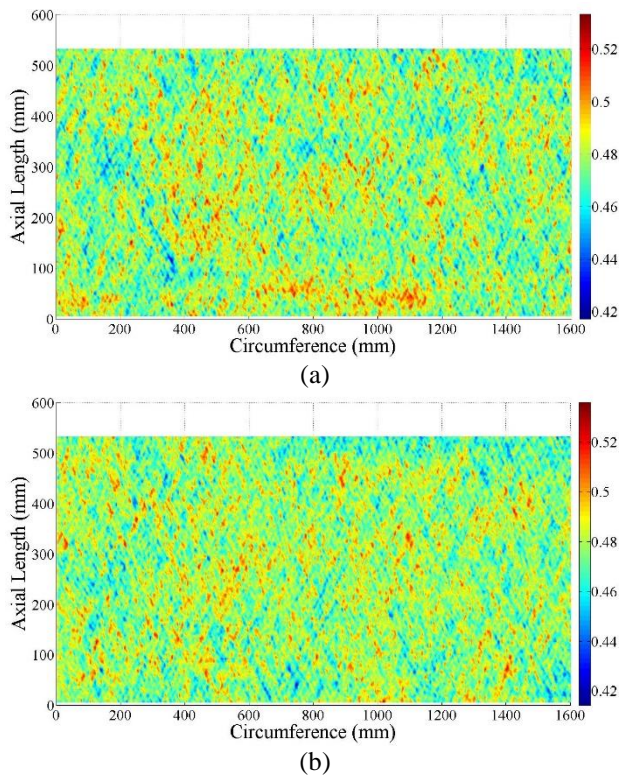


Fig. 13(a) and (b). Examples of matrix imperfections generated from spectral representation method.

5 Monte Carlo Analysis of Ply Gaps and Overlaps

The imperfections in the shell thickness due to ply gaps and overlaps of eight CFRP IM6/8557 UD real cylinders [6] have been successfully isolated using the Hough transform code as evidenced in Figures 3 and 5. Further analyses of these imperfections provide the statistical properties necessary to generate new imperfections for stochastic analysis. The properties of most interest are the variation in the thickness of the lines, the number of lines at various ply angles in any one cylinder and the spatial location of these lines. An example of the ply gaps that were isolated from the Hough transform code are shown in Figures 14(a) and (b).

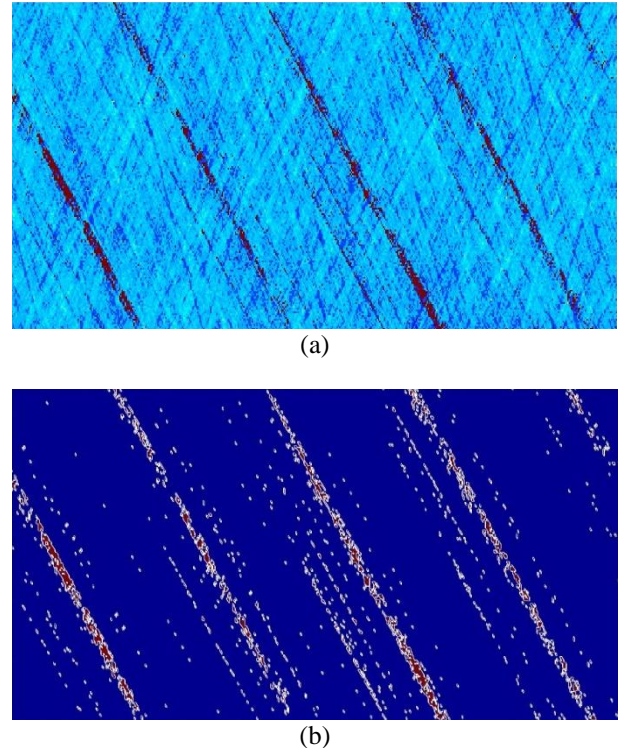


Fig. 14(a) and (b). -41 degree ply gap imperfections from Z17 cylinder [6]. Lowest imperfection points are highlighted in red.

The thickness values of the gap lines were collected and assumed to be normally distributed. Furthermore, as evidenced by Figures 14(a) and (b), the lines of the deepest imperfections are located at almost identical distances from each other. We can take advantage of these patterns to collect the spatial distribution of gap line imperfections on the cylinders for stochastic analysis. First, the lines are rotated so that they are vertical and easy to count.

Next, lines containing 25 or more points are isolated in order to obtain the most prominent ply gaps. The isolated lines represent the spatial areas that ply-gaps are most likely to occur. The precise number of these lines in each of the 8 nominally identical CFRP IM6/8557 UD cylinders [6] were recorded for all ply angles [± 24 , ± 41] and used to construct a Gaussian probability function. Similarly, the spatial distribution of these lines were recorded and utilised to construct a unique probability distribution. Figure 15 features the spatial and thickness probability distribution of the gap lines in the -24 degree direction.

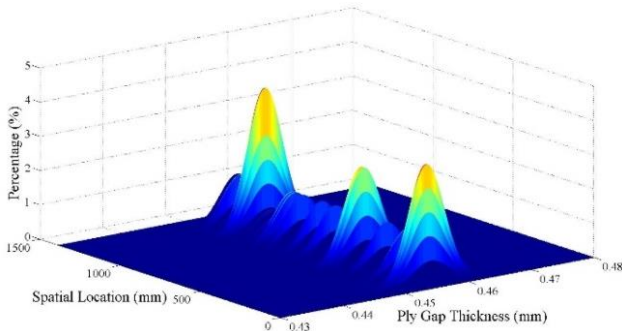


Fig. 15. Probability distribution of -24 degree gap lines.

The thickness of the ply gaps were assumed to be normally distributed about a particular mean and standard deviation which was unique to each ply gap angle. As shown in Figure 18, the spatial location of the ply gaps tend to accumulate at certain locations, with close to 4% of the distributions being localised a certain locations. The localisation of these ply gaps may be attributed to the hand lay-up manufacturing process of the cylinders in which strips of composite plies are arranged side-by-side. A Monte Carlo random number generator was utilised to generate 100 new stochastic fields with variations in ply gap thickness, spatial distribution and quantity that carry the statistical properties of the ply gaps in the original 8 nominally identical shells [6]. An example of a new field is shown in Figure 16.

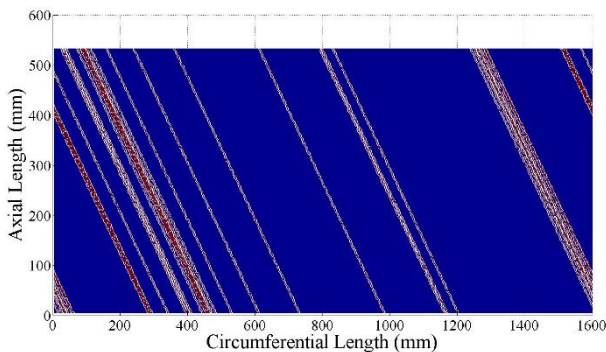
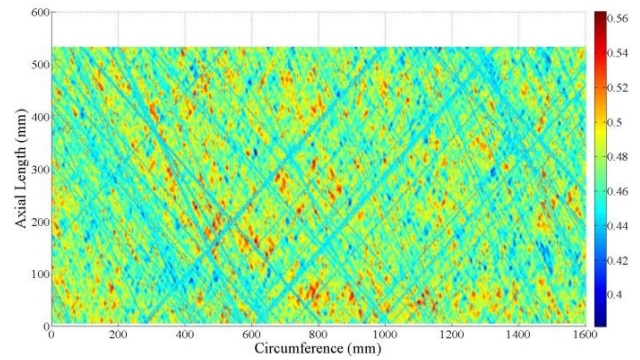


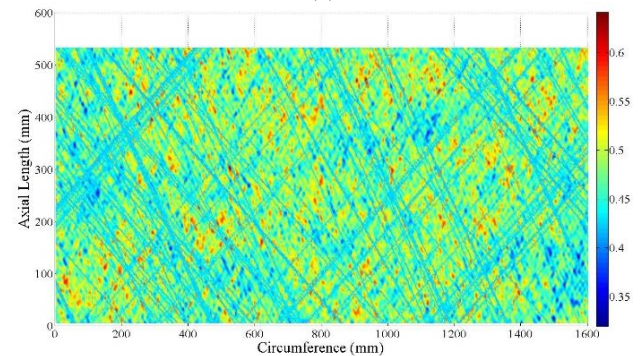
Fig. 16. New field produced with -24 degree ply gaps.

6 Superimposition of Ply Gaps to Matrix Imperfections

Finally, the stochastically generated ply gaps are superimposed onto matrix imperfections that were generated from the spectral representation method. A few examples of the outcome of this process are shown in Figures 17(a) and (b).



(a)



(b)

Fig. 17(a) and (b). Generated thickness imperfections.

7 Conclusion and Future Work

The results generated from the novel method described in this paper are comparable to the original thickness scans provided from DLR [6] shown in Figures 1 and 4. Further analysis and finite element modelling will need to be conducted to ensure the stochastic thicknesses provide modelling results that are similar to the experimental buckling results. Further refinement of the spectrum estimation method and improved STFT windowing functions will provide more accurate stochastic thickness models. The stochastic thickness models may also be used as inputs into the Moving Window Averaging Technique [8-10] to provide stochastically varying imperfect material models.

Acknowledgements

This work was undertaken within the Robust Design of Composite Structures research project of CRC-ACS, established and supported under the Australian Government's Cooperative Research Centres Program and contributes to the European 7th Framework Project DESICOS.

References

- [1] Bushnell D. Buckling of shells – pitfall for designers. *AIAA Journal*, Vol. 19, No. 9, September, 1981.
- [2] W.T. Koiter, *The stability of elastic equilibrium*, Ph.D. thesis, TU-Delft; 1945.
- [3] NASA. Buckling of thin-walled circular cylinders. NASA SP-8007, 1968.
- [4] Hilburger M, Nemeth M, Starnes Jr., J. Shell buckling design criteria based on manufacturing imperfection signatures. *AIAA J.*, Vol. 44, No. 3, pp 654–663, 2006.
- [5] Takano A. Statistical knockdown factors of buckling anisotropic cylinders under axial compression. *Journal of Applied Mechanics*, Vol. 79, 051004, pp 1-17, 2012.
- [6] Degenhardt R, Kling A, Bethge A, Orf J, Kärger L, Zimmermann R, Rohwer K and Calvi A. Investigations on Imperfection Sensitivity and Deduction of Improved Knock-down Factors for Unstiffened CFRP Cylindrical Shells. *Composite Structures*, Vol. 92, No. 8, pp 1939-1946, 2010.
- [7] "DESICOS." DESICOS. Web. 06 July 2013. <http://www.desicos.eu>.
- [8] Broggi M and Schueller G. Efficient Modeling of Imperfections for Buckling Analysis of Composite Cylindrical Shells. *Engineering Structures*, Vol. 33, pp 1796-1806, 2011.
- [9] Broggi M. *Computational Aspects in the Buckling Analysis of Composite Cylindrical Shells with Random Imperfections*. Diss. Leopold-Franzens-Universität Innsbruck. Innsbruck: Leopold-Franzens-Universität Innsbruck, 2011.
- [10] Broggi, M, Schueller G. Accurate prediction of the statistical deviations of the buckling load of imperfect CFRP cylindrical shells. In: *IV European Conference on Computational Mechanics*. Paris, France, EU, 2010.
- [11] Lee M. *Stochastic analysis and robust design of stiffened composite structures*. Diss. The University of New South Wales, 2009. Sydney: UNSWorks, 2009.
- [12] Hühne C, Zimmerman R, Rolfes R, Geier B. Sensitivities to geometrical and loading imperfections on buckling of composite cylindrical shells. Rep. Germany: German Aerospace Centre, Braunschweig, Institute of Structural Mechanics, 2002.
- [13] Hilburger, M and Starnes Jr., J. Effects of Imperfections on the Buckling Response of Compression-loaded Composite Shells. *International Journal of Non-Linear Mechanics* Vol. 37, No. 5, pp 623-43, 2002.
- [14] Alfano, M., and C. Bisagni. Probabilistic Buckling Analysis of Composite and Sandwich Cylindrical Shells. *Proc. of American Institute of Aeronautics and Astronautics SciTech 2014*, National Harbor, Maryland. 2014.
- [15] Schillinger D, Stefanov D and Stavrev A. The Method of Separation for Evolutionary Spectral Density Estimation of Multi-Variate and Multi-Dimensional Non-Stationary Stochastic Processes. *Probabilistic Engineering Mechanics*, 2012.
- [16] Papadopoulos V, and Papadrakakis M. The Effect of Material and Thickness Variability on the Buckling Load of Shells with Random Initial Imperfections. *Computer Methods in Applied Mechanics and Engineering*, Vol. 194, No. 12, pp 1405-426, 2005.
- [17] Schillinger D and Papadopoulos V. Accurate Estimation of Evolutionary Power Spectra for Strongly Narrow-band Random Fields. *Computer Methods in Applied Mechanics and Engineering*, Vol. 199, No.17-20, pp 947-960. 2010.
- [18] Duda R and Hart P. *Use of the Hough Transformation to Detect Lines and Curves in Pictures*. Tech. Vol. 15, Comm. ACM, pp 11-15, 1971.
- [19] Cohen, L. *Time Frequency Analysis: Theory and Applications*. Englewood Cliffs, NJ: Prentice Hall, 1995.
- [20] Spanos P, Tezcan J and Tratskas P. Stochastic Processes Evolutionary Spectrum Estimation via Harmonic Wavelets. *Computer Methods in Applied Mechanics and Engineering*, Vol. 194, No. 12, pp 1367-1383, 2005.
- [21] Stefanou G, and Papadrakakis M. Assessment of Spectral Representation and Karhunen-Loève Expansion Methods for the Simulation of Gaussian Stochastic Fields. *Computer Methods in Applied Mechanics and Engineering*, Vol. 196, No. 21, pp 2465-2477, 2007.
- [22] Schillinger D, Papadopoulos V and Papadrakakis M. Evolutionary Power Spectrum Estimation of Strongly Narrow-Band Random Fields. *Proc. of 2nd South-East European Conference on Computational Mechanics*, Rhodes, Greece, 2009.
- [23] Papoulis A and Pillai S. *Probability, Random Variables and Stochastic Processes*, McGraw-Hill, New York, 2002.

8 Contact Author Email Address

jendi.kepple@unsw.edu.au

Copyright Statement

The authors confirm that they, and/or their company or organization, hold copyright on all of the original material included in this paper. The authors also confirm that they have obtained permission, from the copyright holder of any third party material included in this paper, to publish it as part of their paper. The authors confirm that they give permission, or have obtained permission from the copyright holder of this paper, for the publication and distribution of this paper as part of the ICAS 2014 proceedings or as individual off-prints from the proceedings.